

# Experimental investigation of different geometries of fixed Oscillating Water Column devices

Thomas Vyzikas<sup>a,1</sup>, Samy Deshoulières<sup>b</sup>, Matthew Barton<sup>a</sup>, Olivier Giroux<sup>c</sup>,  
Deborah Greaves<sup>a</sup>, Dave Simmonds<sup>a</sup>

<sup>a</sup> *University of Plymouth, School of Marine Science and Engineering, Drake Circus,  
PL48AA Plymouth, UK*

<sup>b</sup> *Ecole Centrale de Marseille, 38 Rue Frédéric Joliot Curie, 13013 Marseille, France*

<sup>c</sup> *Ecole nationale supérieure des mines de Nantes, 4 Rue Alfred Kastler, 44300 Nantes,  
France*

---

## Abstract

Oscillating Water Columns (OWCs) are some of the most-studied wave energy converters (WECs). Previous work showed that the geometric characteristics of the OWC can play a significant role in the efficiency of the device. In this study, we investigate the behaviour of different designs of OWC making geometric modifications to the classic design of OWC and the U-OWC, initially suggested by Boccotti [1]. The multi-chamber OWCs examined here are fixed on the seabed and have a slit opening at the seaward side. The physical modelling was undertaken in the COAST laboratory of the University of Plymouth. The devices were tested in regular and irregular wave conditions, with and without power take-off (PTO) mechanism, essentially also testing absorbing seawalls. The aim of the study is to present a preliminary comparison related to the geometry of OWCs under some typical wave conditions and suggest potential shape improvements towards an overall optimization of the devices that takes into account both the hydrodynamic efficiency of the OWC and other design aspects, such as the wave run-up. The present study also endeavours to highlight potential benefits from incorporating OWCs in coastal defence as absorbing seawalls.

*Keywords:* OWC, U-OWC, tank testing, hydrodynamic efficiency, geometric

---

<sup>1</sup>Corresponding author, Email address: thomas.vyzikas@plymouth.ac.uk

1 **1. Introduction**

2 As energy consumption increases globally and environmental issues threaten  
3 the quality of life, new sustainable ways of energy generation are actively being  
4 researched. Among them, marine renewable energy (MRE) appears to be a vi-  
5 able alternative [2]. MRE includes various technologies, such as wave, tidal, off-  
6 shore wind and thermal energy. At the moment, only offshore wind power and,  
7 to a lesser extent, tidal power are considered mature technologies and receive  
8 sufficient investments. On the other hand, emerging wave energy technologies  
9 are currently not economically competitive, but still attract engineering inter-  
10 est thanks to the high power density of sea waves and its potential exploitation  
11 [3]. In the recent past, the wave energy industry has faced important failures  
12 that have delayed the expansion of these technologies. For example, the device  
13 installed in Toftestallen was destroyed by a storm in 1998 after six years of  
14 good operation [4]. The hybrid pier in Mutriku faced serious damages by severe  
15 storms (2007-2009), mainly at uncompleted OWCs [5], possibly due to the non-  
16 monolithic design of the chambers and imperfections at the construction stage  
17 [6]. After maintenance and modifications though, the Mutriku plant is a good  
18 working example of the OWC technology, covering the needs of 100 households.  
19 Moreover, the icon of the MRE industry, "Pelamis", went to administration in  
20 late 2014, having issues securing funding for future developments. It became  
21 clear that research is needed for creating robust and efficient devices, in order to  
22 boost the development of the wave energy industry [7] and to identify collateral  
23 benefits of the use of MRE technologies in sea defences.

24 Out of the hundreds of patents of WECs registered worldwide, OWC tech-  
25 nology appears to be one of the most successful, reaching the stage of full-scale  
26 prototypes [8] [9]. On the one hand, there are offshore devices located in deep  
27 water, where the available wave power is relatively high. These offshore OWCs  
28 are in general floating devices, developed for the first time by Masuda and

29 commercialized in Japan in 1965 [10]. The first theoretical model of a floating  
30 OWC was established by McCormick [11] and recently a 1:4<sup>th</sup>-scale buoy con-  
31 verter was deployed in Galway Bay, Ireland [12]. On the other hand, there are  
32 onshore devices located along the coast in shallow water that are exposed to  
33 lower energy potential, unless there are some local energy focusing effects, e.g.  
34 due to topography. In fact, around 70% of the energy available in deep water  
35 waves is lost through bottom friction as the waves approach the shore [13]. How-  
36 ever, onshore or nearshore OWCs have some advantages compared to offshore  
37 OWCs: *i*) mooring lines and wet power-transmission cables are not required,  
38 *ii*) they operate in a safer sea environment, which increases their survivability,  
39 *iii*) they can be more easily accessed and maintained and *iv*) they can serve a  
40 dual purpose: electricity generation and coastal protection [14]. The latter is  
41 a considerable advantage for OWCs embedded in breakwaters, since the added  
42 benefits will increase the viability of such a project by setting a cost-sharing  
43 basis.

44 In its classic form, an onshore OWC system consists of a partially submerged  
45 hollow structure, where an underlying water column coexists with an overlying  
46 air one, which is connected to the atmosphere with a duct. A submerged seaward  
47 opening allows water to flow into the OWC causing internal water oscillation.  
48 Subsequently, the water oscillation drives the motion of air and energy can be  
49 converted to useful power through a PTO mechanism, usually in the form of  
50 a bi-directional air turbine placed in the duct, e.g. Wells turbine. An alter-  
51 native to the conventional OWC is the U-OWC device [1], which incorporates  
52 an additional seaward wall. The U-shape structure appears to be more efficient  
53 than the classic OWC shape for realistic sea states, where wind waves and swells  
54 coexist, without the need of latching control. As a consequence, the U-OWC is  
55 able to resonate in greater frequency bandwidth than the original OWC.

56 OWC devices have been examined extensively with physical, theoretical,  
57 and numerical models. Some milestone experimental studies of OWCs can be  
58 found in the literature [15] [16] that are commonly used for comparisons and  
59 validation of numerical models in more recent studies [17] [18] [19]. Other

60 benchmark studies were undertaken by Evans & Porter [20], who developed a  
61 theoretical model based on potential theory, to explore the interaction of an  
62 OWC with incident waves and to determine its hydrodynamic efficiency. An  
63 analytical description of a U-OWC under the assumption of linear wave theory  
64 was suggested by Boccotti et al. [21] and was further developed to include  
65 a more accurate description of the wave field and the dynamics of the device  
66 [22]. Advanced experimental studies of OWCs employed the particle image  
67 velocimetry (PIV) technique for acquiring better insight into the hydrodynamics  
68 of the OWC [23] [24] and the air motion in the chamber [25]. Commonly, recent  
69 work focuses upon the need for validation of numerical models, such as spectral  
70 models [26] or computational fluid dynamic (CFD) solvers [27] [28] [29], and the  
71 acquisition of appropriate experimental datasets for that scope.

72 Recognizing the important steps taken by Boccotti [30] in achieving im-  
73 proved performance via geometric optimization of OWCs, the experimental work  
74 presented here examines four different OWC geometries, which consist of three  
75 rectangular chambers and have alternative external design. The behaviour of  
76 these OWCs is investigated in regular and irregular wave conditions, showing  
77 how the suggested modifications influence the performance of the devices, the  
78 oscillation of the water columns, the run-up on the front wall and the relative  
79 motion in the individual chambers. The scope of the work is to show an initial  
80 qualitative comparison between the four devices in some typical wave conditions.  
81 A companion study referring to the validation of the CFD model OpenFOAM  
82 using the present datasets can facilitate the examination of the hydrodynamic  
83 characteristics of the OWCs in more detail [31].

84 In the present study, the devices were tested with and without PTO, since  
85 OWCs can potentially operate as absorbing seawalls offering additional advan-  
86 tages to the classic coastal protection structures [32]. The possible merits of  
87 using OWC embedded in breakwaters include reduced wave run-up and use of  
88 less material for the construction of caissons. However, the high level of noise  
89 produced by the turbine is usually a serious consideration for using OWCs near  
90 inhabited areas and touristic marinas [6]. Also, the cost of the mechanical and

91 electrical equipment, regarding the turbine system, cannot be considered in-  
92 significant, affecting the attractiveness of the devices to new investors. In the  
93 current stage of development of MRE, even prototypes without PTO might be  
94 helpful in gaining engineering experience to avoid future failures.

95 In the remainder of the paper, the description of the devices and the exper-  
96 imental conditions are presented in Section 2. The experimental results for the  
97 four devices and the different wave conditions are shown in Section 3. Finally,  
98 conclusions and suggestions for future work are drawn in Section 4.

## 99 **2. Laboratory Methodology**

### 100 *2.1. Models' design*

#### 101 *2.1.1. Four variants of OWC*

102 As mentioned in the introduction, the tests reported here focus on four  
103 variants of three-chamber OWC models with and without a PTO, which are  
104 hereafter referred as “lid-on” and “lid-off” models, respectively. The PTO is  
105 simulated by a lid with a circular orifice. The schematic of the four variants  
106 shown in Figure 1 illustrates the common characteristics of the devices, which  
107 are the internal dimensions of the OWC, in particular the width of the chamber  
108 and the height of the air column, and the size of the orifice, which causes the  
109 same damping for all the lid-on cases.

110 *Model 1:* After studying many different concepts [1] and after parametric  
111 optimization [21] [33], Boccotti proposed an improved design of an OWC that  
112 has greater resonant bandwidth thanks to its U-shape, allowing it to exploit the  
113 energy of both swells and wind waves [30]. A small-scale prototype of this device  
114 was tested also in field conditions at the Natural Ocean Engineering Laboratory  
115 (NOEL) [34] and full-scale models are under construction in Civitavecchia port  
116 [35]. Two other projects have also been approved for the Marina di Cicerone  
117 and the Commercial port of Salerno. In the present study, the configuration of  
118 the U-OWC tested in NOEL was adopted [34], representing Model 1 in Figure  
119 1.

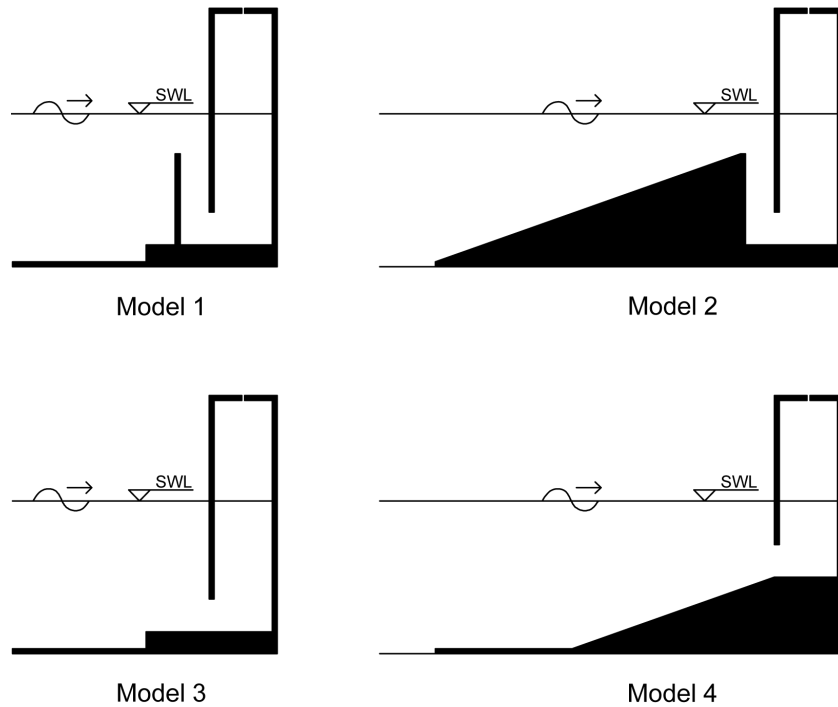


Figure 1: The four lid-on devices studied in the experimental tests. \*SWL=still water level

120 *Model 2*: This model in Figure 1 resembles the U-shape of Boccotti’s design  
 121 [34], but it is fronted by a submerged slope representing part of the toe or  
 122 armour section of a real breakwater. This slope has a gradient of 1:2.5, which is  
 123 a typical value for rubble-mound breakwaters, and it expands from the highest  
 124 point of the submerged wall to the seaward side. The scope of this modification  
 125 is to examine the impact of an armoured slope or a toe protection structure  
 126 on the hydrodynamic characteristics of the OWC. Realistic studies of OWCs  
 127 should consider such a sloping structure in front of the main structure for toe  
 128 protection, especially because WECs are designed to operate in energetic sea  
 129 climates. In any case, sediment transport and debris accumulation tend to  
 130 create inclined features on the bed in front of such structures over long periods  
 131 of time [36].

132 *Model 3*: This model refers to the conventional design of the OWC shown as

133 Model 3 in Figure 1. It is probably the device with the simplest geometry, com-  
134 prising a vertical seaward wall with a horizontal slit opening at the bottom. This  
135 type of device has been extensively studied experimentally [16] and numerically  
136 [37], as mentioned in the Introduction. Prototypes have also been constructed  
137 and operated in sea for a number of years, such as the PICO [9] and LIMPET  
138 device [8]. Compared to previous studies [27] [17], the present work examines  
139 conventional OWCs with higher draught of the front wall and high damping.  
140 This geometry was considered in order to be consistent with Boccotti’s design  
141 of the U-OWC [34] and allow for direct comparisons to be drawn. The high  
142 damping in combination with the relatively high waves tested here results in  
143 high air pressure in the OWC chambers, making the present study challenging.

144 *Model 4:* An alteration of the conventional design, referred to as Model 4  
145 in Figure 1, was also examined following the same principles of toe protection  
146 as for Model 2. A similar configuration has been tested in approximately 1:6<sup>th</sup>  
147 of the present scale by Koola et al. [38]. Model 4 has a shorter draught of the  
148 seaward wall, but the same slit opening as Model 3. Note that, the bottom of  
149 the chambers is raised inside the OWC, so that it is at half of the water depth,  
150 similar to the conventional OWC model suggested by Boccotti [30]. The slope  
151 in front of the device is again 1:2.5. The scope of testing Model 4 is to examine  
152 the influence of a different draught, keeping the seaward slit opening constant.  
153 At the same time, the effect of the toe protection can be examined through  
154 comparison with Model 3.

### 155 2.1.2. Model scaling

156 The 35m long flume of the COAST laboratory at the University of Plymouth  
157 [39], where the experiments took place, has a maximum operational depth of  
158 0.75m and width of 0.6m. The flume is equipped with an absorbing piston-type  
159 wave paddle that is capable of generating regular and irregular waves. The  
160 OWCs were placed before the other end of the flume with the back wall of  
161 the structure at a distance of 28m from the wave paddle. All the walls of the  
162 flume are transparent allowing visual observations. The experimental set-up is

163 presented in Figure 4.

164 The scaling of the present model was based on the water depth ratio between  
 165 Boccotti’s small-scale field experiments [34] and the maximum available water  
 166 depth of COAST’s flume. Boccotti’s model was located at a water depth of  
 167 2.1 m, therefore the model had to be scaled down to fit into the depth of 0.75  
 168 m of the present flume. The OWC was scaled by Froude dynamic similarity  
 169 [40], since gravity waves are examined with wavelengths much larger compared  
 170 to the wave heights and the viscous forces on water surface motion inside the  
 171 device are small. Therefore, the geometric scaling factor obtained from the two  
 172 water depths is:

$$s_f = \frac{\text{Length of prototype}}{\text{Length of model}} = \frac{2.1}{0.75} = 2.8 \quad (1)$$

173 Based on  $s_f$ , the scaled geometric characteristics of the OWCs are listed  
 174 in Table 1. The parameters of this Table are shown in the generic schematic  
 175 of the devices, referring to Model 1, in side view (Figure 2) and plan view  
 176 (Figure 3). It can be seen that the OWCs are symmetrical to the centreline  
 177 of the flume, and thanks to this symmetry, 2-dimensional tests in a flume can  
 178 be conducted for uni-directional waves. The devices were manufactured from  
 179 marine plywood with all the intersections bonded and sealed with silicon filler  
 180 for ensuring airtightness.

$h_d$	$w_1$	$w_2$	$w_3$	$s_o$	$c_1$	$c_2$
0.750	0.554	0.518	0.107	0.161	0.644	2.000
$b_1$	$b_2$	$k_w$	$o_r$	$l_1$	$l_{tot}$	
0.143	0.286	0.024	0.015	0.184	0.600	

Table 1: Size of geometric parameters of the present OWC device in (m).

### 181 2.1.3. Power Take-Off

182 The conversion of the pneumatic energy of the air in the OWC chambers  
 183 to electricity is performed by a PTO mechanism, which in the case of OWCs,



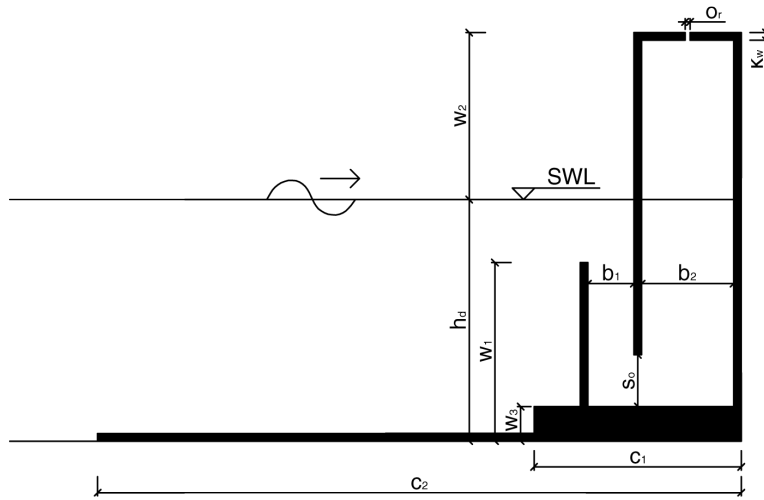


Figure 2: Side view of the U-OWC with the geometric parameters used.

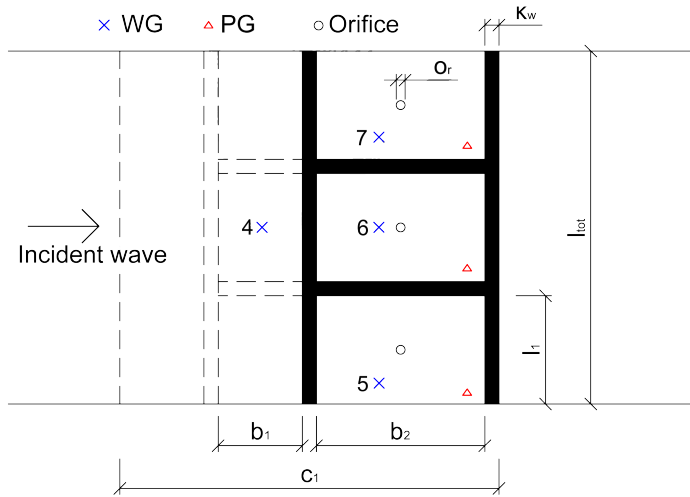


Figure 3: Plan view of the experimental model displaying the locations of the pressure gauges (PG), wave gauges (WG) and orifices.

184 is usually a bi-directional Wells turbine [41]. Due to scaling differences and  
185 modelling difficulties in the laboratory, a scaled turbine is not usually practical.  
186 However, its damping effect has to be reproduced, since it alters the hydrody-  
187 namic behaviour of the device. Using an orifice is a well-established method  
188 for that scope [42] [43]. The size of the orifice determines the magnitude of the  
189 damping. In the present study, a circular orifice was placed in the lid at the top  
190 of each chamber of the OWC. Its diameter of 1.5 cm was scaled on Boccotti's  
191 design [34] to achieve an orifice of 0.35% of the total plan area of each chamber.  
192 All the OWC variants were tested with the same circular orifices, as shown in  
193 Figure 3. The damping due to the small orifice is higher compared to similar  
194 previous studies, where the orifice covered 2.7% - 14.7% [28], 0.78% - 7.8% [43]  
195 and 0.78% - 3.91% [27] of the plan area of the chamber, resulting in significant  
196 internal air pressure.

197 The same devices were tested without a PTO by completely removing the  
198 lid. The lid-off results can only be used for examining absorbing seawalls and  
199 not WECs, since the inclusion of a PTO alters the eigenfrequency of the device  
200 and consequently its hydrodynamic response and performance. Nonetheless,  
201 the comparison between OWCs with and without PTO presented in Section  
202 3 reveals interesting information regarding the wave dissipation and general  
203 behaviour of the devices for potential other uses as elements of breakwaters..

## 204 *2.2. Experimental design*

### 205 *2.2.1. Instrumentation and data acquisition*

206 The free surface elevation was recorded with seven resistive wave gauges  
207 (WG) at a sampling frequency of 128 Hz. After testing each model, the WGs  
208 were recalibrated for greater confidence. Between the wave tests, the free sur-  
209 face was allowed to settle for approximately five minutes, in order to avoid any  
210 spurious effects from long or cross-shore waves remaining in the flume. The  
211 positions of the WGs are shown in Figures 3 and 4, with WGs 1-4 located up-  
212 stream of the OWCs along the flume centreline and WGs 5-7 placed inside each  
213 one of the three chambers. The first three WGs were used to measure the inci-

214 dent waves for quality control of the results and later for the reflection analysis  
 215 (see Section 3.2.1). WG 4 was used to measure the water elevation just in  
 216 front of the devices, which is practically associated with the run-up on the front  
 217 wall of the OWCs. WGs 5-7 were placed at different offsets from the side walls  
 218 of each chamber (see Figure 3), in order to examine the possibility of internal  
 219 waves (sloshing) or disturbances inside the chambers, by comparing the phase  
 220 differences from the recordings. Of course, sloshing can be observed better  
 221 with more than one WG in the same chamber, but thanks to the symmetry of  
 222 the chambers, the present layout of the WGs allows for such studies.

223 For the lid-on tests, a pressure gauge (PG) was mounted on the lid of each  
 224 chamber to measure the pressure variations in the chamber, as shown in Figure  
 225 3. The recorded pressure was used for the calculation of the power absorbed  
 226 and capture width of the device. The sampling frequency of the PGs was also  
 227 128Hz and the recording was synchronised with the WGs.

228 The wave generation was performed by a piston wave paddle, which was  
 229 computer-controlled with a linear transfer function. Absorption was achieved  
 230 through a force feedback mechanism [44]. A ramp-up time of approximately  
 231 one wave period was selected at the paddle control to facilitate the smooth  
 232 generation of the first waves in still water.

233 To assess the laboratory errors, a repeatability evaluation was performed  
 234 using regular waves and Model 1. Each test was repeated five times with Model  
 235 1 lid-on. The first test was used as a reference measurement and the error for

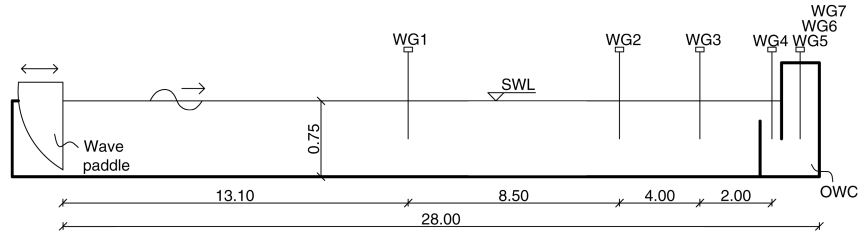


Figure 4: Experimental set-up indicating the locations of the wave gauges (WG) relative to the OWC and the wave paddle. Dimensions in (m).

236 each test was calculated as the mean value of the absolute difference between  
 237 the corresponding peaks of the two examined timeseries over the wave height,  
 238 as seen in Equation 2. The wave height is calculated as the mean value of the  
 239 difference between the elevations of the crests and the neighbouring troughs  
 240 recorded in the windowed timeseries after the ramp-up waves and before the  
 241 arrival of reflections. The total error for each wave is calculated as the mean  
 242 value of the errors from the four comparisons with first test. The average error  
 243 for all the regular wave tests was approximately 1%, indicating that the results  
 244 are consistent and repeatable.

$$Error = \frac{1}{N} \sum_1^N \frac{|recording\ 1 - recording\ i|}{wave\ height} 100\% \quad (2)$$

### 245 2.2.2. Wave characteristics

246 The four devices were tested with and without PTO under four regular and  
 247 four irregular wave conditions. The characteristics of the regular waves are  
 248 shown in Table 2, referring to the analysed values from the obtained timeseries  
 249 with  $H$  and  $f$  being the wave height and frequency, respectively. For each  
 250 wave, the recorded signal from WGs 1-3 was windowed to remove the ramp-up  
 251 of the paddle and the reflections from the OWC. This method is preferred for  
 252 determining the incident wave characteristics, instead of using the input values  
 253 to the wave paddle, because it eliminates any potential discrepancies induced  
 254 by the calibration and it provides more accurate input for the calculations that  
 255 follow.

256 The initial selection of the waves was based on the natural frequency of  
 257 the OWC, which can be estimated from the draught of its front wall [45], as  
 258 seen in Equation 3. According to Equation 3, the natural frequency of Model  
 259 3 is approximately 0.51 Hz. It was decided to examine two other lower wave  
 260 frequencies and a higher wave frequency, in order to cover sufficient frequency

261 bandwidth.

$$f_c = \frac{1}{2\pi} \sqrt{\frac{g}{L_1 + L_2}} \quad (3)$$

262 where  $L_1$  is the draught of the front wall of the OWC and  $L_2$  is an effective  
 263 length due to the added mass induced by the PTO, here approximated as equal  
 264 to  $L_1$ .

265 Each regular wave test had a duration of 30 s, essentially assessing 4-7 wave  
 266 periods, depending on the case. For the given water depth, these heights and  
 267 periods correspond to intermediate depth second order waves [46]. The range  
 268 of wave periods and heights was selected in order to examine waves around the  
 269 resonant frequency of the OWCs, with different steepness.

Wave	Regular waves		Irregular waves	
	$H$ (m)	$f$ (Hz)	$H_s$ (m)	$f_p$ (Hz)
1	0.122	0.570	0.066	0.651
2	0.096	0.510	0.057	0.602
3	0.088	0.465	0.056	0.551
4	0.159	0.385	0.077	0.445

Table 2: Regular and irregular wave characteristics

270 The wave characteristics of the four irregular waves tested are also shown  
 271 in Table 2, with  $H_s$  and  $f_p$  being the significant wave height and peak period  
 272 of the measured spectrum in the flume, respectively. A Joint North Sea Wave  
 273 Project (JONSWAP) [47] energy spectrum was chosen as an input spectrum at  
 274 the wave paddle, since this type of spectrum represents a widely used energy  
 275 distribution in industry. Its equation relating  $H_s$  and  $f_p$  is given in Equation  
 276 4 and it can be derived from the basic equation [46] using  $H_s = 4\sqrt{m_0}$  and  
 277  $m_0 = \alpha g^2 \omega^{-4} (0.06533\gamma^{0.8015} + 0.13467)$ , with  $m_0$  being the zeroth moment of

278 the spectrum and  $\alpha$  a spectral parameter.

$$S_{jon}(f) = 0.205H_s^2 f_p^4 f^{-5} \exp\left(-\frac{5}{4}\left(\frac{f_p}{f}\right)^4\right) \gamma^r \quad (4)$$

279 where  $f$  is the discrete frequency of each wave component,  $\gamma$  ( $= 3.3$ ) the  
280 JONSWAP spectral peak enhancement parameter and  $r = \exp[-\frac{(f-f_p)^2}{2f_p^2\sigma^2}]$ , with  
281  $\sigma = 0.07$  for  $f \leq f_p$  or  $\sigma = 0.09$  for  $f > f_p$ .

282 The energy spectrum was generated by the wave paddle with linear super-  
283 imposition of 200 wave components with assigned random phases between 0 and  
284  $2\pi$  rad. A low and high cut-off frequency corresponding to 0.2 Hz and 1.5 Hz,  
285 respectively were used to limit the wave generation to wave components with  
286 meaningful energy only. The repeat interval of the signal was 180 s.

287 The values for irregular waves in Table 2 were obtained after analysing the  
288 recorded timeseries of the surface elevation by means of reflection analysis, as  
289 described in Sections 3.2.1 and 3.2.2. These values were selected in order to  
290 correspond to relatively mild wave condition in the South West of England [48]  
291 and to have  $f_p$  close to the resonance frequency of the examined OWCs. The  
292  $H_s$  and  $f_p$  values were scaled based on the water depth, taken as 10 m in full  
293 scale, using Froude similarity with a scale of approximately 1:13.

### 294 **3. Results and discussion**

#### 295 *3.1. Regular waves*

##### 296 *3.1.1. Relative surface elevation at characteristic locations*

297 The results of the surface elevation are examined at two characteristic loca-  
298 tions of the OWC, namely inside the central chamber and at the front wall, mea-  
299 sured with WG 6 and WG 4, respectively. The surface elevation is normalised  
300 by the incident wave height and it is used here to observe the general response  
301 of the OWC models, useful for the design. Commonly, the non-dimensional Re-  
302 sponse Amplitude Operator (RAO) is employed, which is defined for one degree

303 of freedom, i.e. vertical oscillation, by the non-dimensional ratio of amplitudes  
 304 without considering the phases [49] as:

$$RAO(f) = \frac{\Xi}{\alpha_w} \quad (5)$$

305 where  $\Xi$  represents the amplitude of the response of the water surface in  
 306 the chamber of the OWC and  $\alpha_w$  the amplitude of the incident wave, which, to  
 307 good approximation, is taken as half of the wave height ( $H$ ).

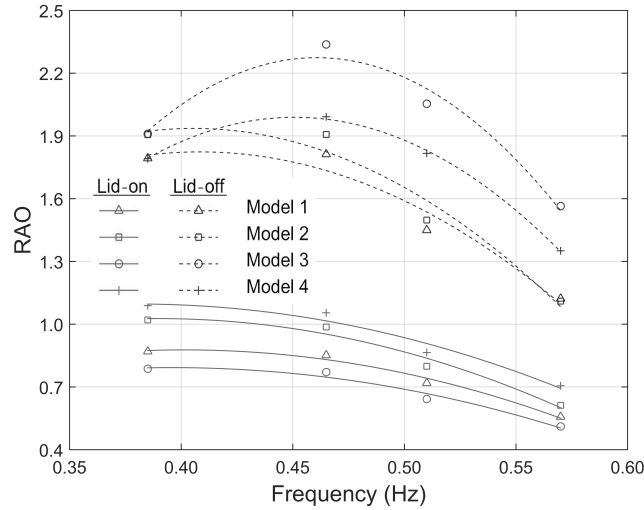


Figure 5: Relative surface elevation inside the central chamber of each lid-off (- -) and lid-on (-) device for the four regular wave conditions.

308 Figure 5 presents the RAO in the central chamber of each device for the  
 309 lid-on and lid-off configurations for the four regular waves tested. A second  
 310 order polynomial fitting is plotted to facilitate comparison of the results. The  
 311 central chamber is selected as a representative case, since for most of the waves  
 312 and devices tested, the behaviour of the three chambers is similar, as discussed  
 313 in Section 3.1.3.

314 The effect of the damping induced by the PTO can be clearly observed, since  
 315 the RAO of the lid-on OWCs is around half that of the lid-off OWCs, as might be  
 316 anticipated. Moreover, the shape of the curves indicates a possible resonance

317 at approximately 0.45 Hz for the lid-off models and at a lower frequency for  
 318 the lid-on models. However, this is hard to confirm due to the limited range  
 319 of the frequencies examined. It can be seen that Equation 3 with  $L_1 = L_2$   
 320 overestimates the resonant frequency of the OWCs, possibly due to the high  
 321 damping of the PTO, which results in greater added mass.

322 An interesting observation from Figure 5 refers to the relative behaviour of  
 323 the four models, which is substantially different between the lid-on and lid-off  
 324 cases. The conventional design (Model 3) appears to have the highest RAO  
 325 in the absence of lid and the lowest when the lid is present. The same trend  
 326 appears for Model 4, which is a modification of Model 3. On the other hand,  
 327 Models 1 and 2 have the two lowest RAO for the lid-off configuration and the  
 328 two highest for the lid-on configuration. This indicates that the extra submerged  
 329 seaward wall of U-OWCs significantly alters the hydrodynamic behaviour of the  
 330 device compared to the conventional OWCs. Another important observation is  
 331 that the U-OWC with the ramp (Model 2) has higher RAO compared to the  
 332 standard U-OWC, irrespectively of the presence of the lid.

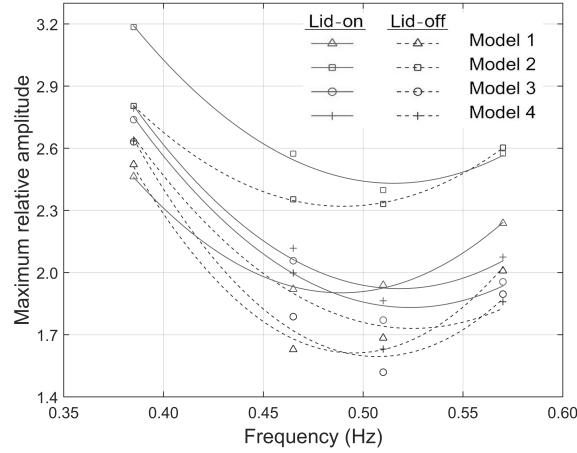


Figure 6: Relative surface elevation at the front wall (WG 4) of each lid-off (- -) and lid-on (-) device for the four regular wave conditions.

333 The second characteristic location refers to WG 4 upstream of the front



334 wall of the OWCs, which can be used to examine the run-up on the front wall.  
 335 Figure 6 shows the run-up for all the lid-on and lid-off devices under the four  
 336 regular wave conditions, normalized by the incident wave amplitude. Run-up is  
 337 calculated as the average of the maxima of surface elevation recorded in every  
 338 wave test. A second order polynomial fitting is plotted for ease of comparisons.

339 In general, Figure 6 shows that the run-up is higher for the lid-on cases when  
 340 examining a specific device. Additionally, Model 2 has significantly higher run-  
 341 up compared with the other models, which is presumed here to be an effect  
 342 the shoaling caused by the ramp. The same can be observed for Model 4 when  
 343 compared to Model 3, but since the draught of the front wall is different and the  
 344 slope is shorter, no immediate conclusion should be drawn. The conventional  
 345 U-OWC (Model 1) has small run-up for the low-frequency waves only, while  
 346 the conventional OWC (Model 3) induces low run-up for the whole range of  
 347 frequencies tested.

348 Run-up might be an important restriction when designing marinas and ports,  
 349 causing operational problems in cases of over-topping. The run-up on a fully  
 350 reflective vertical breakwater is approximately two times the incident wave am-  
 351 plitude. Thus, for the majority of the tests in Figure 6, excluding Model 4  
 352 and the lowest-frequency wave, a breakwater with embedded OWCs should be-  
 353 have better than a conventional vertical breakwater, with lower likelihood of  
 354 over-topping.

### 355 3.1.2. Hydrodynamic efficiency

356 The most important parameter when examining the performance of an OWC  
 357 is the hydrodynamic efficiency, which is defined as the ratio of the power ab-  
 358 sorbed by the OWC ( $P_{abs}$ ) over the incident wave power ( $P_{inc}$ ) per meter width  
 359 of the device, as seen in Equation 6. The hydrodynamic efficiency is also referred  
 360 in the literature as capture width ratio ( $C_w$ ) [45], and of course it is calculated  
 361 for devices with PTOs only.

$$C_w = \frac{P_{abs}}{P_{inc}} \quad (6)$$

362 The incident wave power is given by the total incident energy, i.e. the  
 363 summation of kinetic and potential energy, per time unit and per meter length  
 364 of the wave crest, as shown in Equation 7 [45]:

$$P_{inc} = \frac{1}{8} w \rho g H^2 c_g \quad (7)$$

365 where  $w$  the transverse width of the wave tank, which corresponds here  
 366 to thwidth of the chambers ( $l_1$  in Table 1),  $\rho$  the density of the water,  $g$   
 367 the gravitational acceleration and  $c_g$  the wave group celerity, given as  $c_g =$   
 368  $\frac{\omega}{\kappa} \frac{1}{2} \left( 1 + \frac{2\kappa h}{\sinh(2\kappa h)} \right)$ , with  $\omega$  being the angular frequency of the wave,  $h$  the depth  
 369 of the flume and  $\kappa$  the wave number.

370 For the calculation of the power absorbed by the OWC, the timeseries of  
 371 the free surface displacement and pressure are required. The power absorbed  
 372 by the device is calculated by the energy absorbed in one wave cycle divided by  
 373 the wave period ( $T$ ), as shown Equation 8:

$$P_{abs} = \frac{1}{T} \int_0^T p(t) v(t) S_c dt \quad (8)$$

374 where  $p(t)$  the instantaneous air pressure inside the chamber and  $v(t)$  the  
 375 instantaneous velocity inside the chamber, calculated by the time derivative of  
 376 the free surface displacement in the device.  $S_c$  is the section of the chamber,  
 377 given by its internal dimensions, namely  $b_2 \times l_1$  (see Table 1).

378 Figure 7 presents the hydrodynamic efficiency of the four devices under the  
 379 four regular conditions, calculated from the recordings in the central chamber. A  
 380 second order polynomial fitting is also used for easier comparisons. Considering  
 381 the shape of the curves and the large variation of  $C_w$ , it seems that the waves  
 382 tested cover the frequency region around the maximum performance of the  
 383 devices, which gives added value to the present results.

384 The results of Figure 7 are somewhat comparable with those for the RAO  
 385 of the lid-on devices in Figure 5, confirming that the presence of the ramp  
 386 alters the hydrodynamics of the OWCs and improves the performance, since  
 387 Model 2 and Model 4 have higher values of  $C_w$  than Model 1 and Model 3,

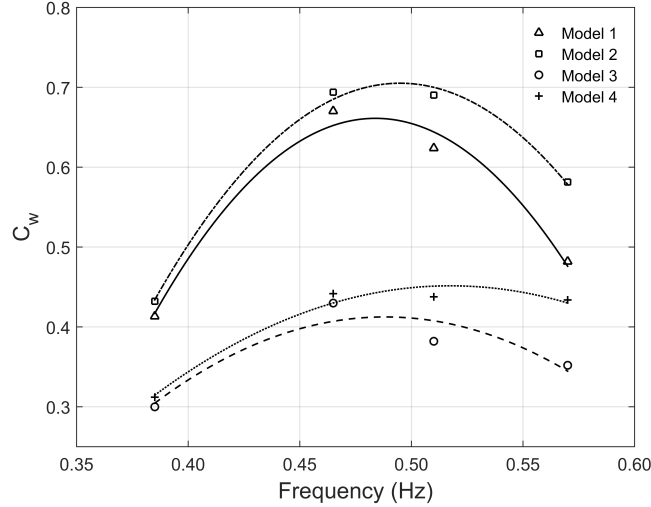


Figure 7: Capture width for the central chamber of each device for the four regular waves.

388 respectively. The most important aspect of the results regarding the  $C_w$ , is  
 389 the significant improvement in the performance of U-OWCs (Models 1 and 2)  
 390 compared to conventional OWCs (Models 3 and 4), especially close to the peak  
 391 of the performance curve, where  $C_w$  is almost twice as high.

### 392 3.1.3. Comparison between the chambers

393 As stated in Section 2.1 all the OWC devices had three identical chambers,  
 394 which were not connected. Therefore, the chambers are expected to respond  
 395 independently to the incident waves and in theory, they should have identical  
 396 behaviour. Here, the relative response of the three chambers of the lid-off devices  
 397 is examined for all the regular waves. The comparison between the chambers is  
 398 performed by means of RAOs, similar to the analysis in Section 3.1.1. The lid-  
 399 off devices are selected for this test, because they have higher RAOs compared  
 400 to the lid-on devices and their results are not influenced by imperfections in the  
 401 manufacturing of the lid.

402 The results are shown in Figure 8, where the markers indicate the different  
 403 models and the colours refer to each of the four regular waves. If a line is

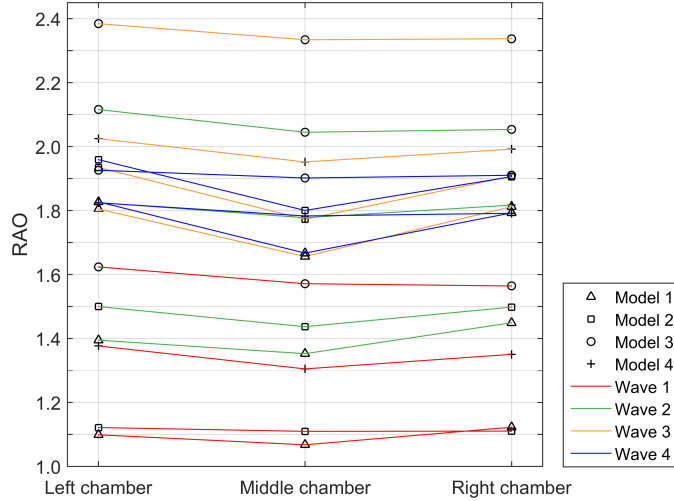


Figure 8: RAO of the three chambers for the lid-off devices under the four regular waves.

404 horizontal, the chambers behave exactly the same. The left, middle and right  
 405 chamber here refer to the bottom, central and top chambers in Figure 3, with  
 406 recordings taken from WG 5, WG 6 and WG 7, respectively. The present results  
 407 indicate that the behaviour of the three chambers is not identical. It should be  
 408 noted that this does not seem to be an effect of the layout of the internal WGs,  
 409 which were located in such a way (see Figure 3), in order to observe possible  
 410 sloshing or any other disturbances of the free surface inside the chambers. The  
 411 examination of the timeseries of the surface elevation showed that the internal  
 412 oscillation had the same phase for all the three WGs in the chambers.

413 In particular, the behaviour of the three chambers is similar for Wave 1 and  
 414 it has more discrepancies for Wave 4, which indicates that there is a potential  
 415 correlation between the wave length and the differences in RAO between the  
 416 chambers. Moreover, Models 1 and 2 seem to have noticeably higher RAO of  
 417 the side chambers compared to the central one, especially for the longer waves  
 418 (Waves 3 and 4). The same is not the case for Models 3 and 4, where the  
 419 behaviour of the chambers is more consistent. This indicates that the presence

420 of the submerged wall of the U-OWCs alters the hydrodynamic characteristics  
421 of the flow and results in different RAOs for the chambers. One can argue  
422 that the side walls of the flume can potentially alter the behaviour of the side  
423 chambers in comparison to the central one, but despite the fact that the problem  
424 is symmetrical, these chambers did not exhibit always consistent behaviour for  
425 all the cases tested here. Further examination of the flow patterns in the vicinity  
426 and inside the devices is required for explaining the different behaviour of the  
427 chambers.

### 428 *3.2. Irregular waves*

#### 429 *3.2.1. Data processing*

430 The analysis of irregular waves with random phases requires special pro-  
431 cessing of the results in order to remove the reflections and create a smooth  
432 spectrum, which is easier to interpret.

433 During the 180 s of each irregular wave test, there are many reflected waves  
434 from the OWC and some re-reflected waves from the wave paddle, which con-  
435 taminates the recorded signal. The accurate assessment of the performance of  
436 the devices requires the extraction of the incident wave field from the measured  
437 timeseries. This can be achieved by means of reflection analysis. A two-WG  
438 method [50] was employed here, using the recordings of the surface elevation  
439 from WG 2 and WG 3. This option was considered the best, since the dis-  
440 tance between WG 1 and WG 2 is much longer and WG 4 is subject to local  
441 flow disturbances caused by the OWC. Common practice suggests short dis-  
442 tance between the WGs used for reflection analysis of approximately 10-20 cm.  
443 However, trial of the method to synthetic data and numerical model results [31]  
444 demonstrated that even for much longer distances between the WGs, e.g. 1-4 m,  
445 the shape and the energy of the incident spectrum can be accurately predicted.  
446 Increasing the distance between the WGs mainly affected the phasing of the  
447 wave components, resulting in discrepancies in the observed surface elevation.

448 The estimation of the spectral properties was achieved through segmentation  
449 and averaging of the spectrum obtained after the reflection analysis, in order

450 to yield a smoother spectrum for better interpretation of the results [46]. This  
451 is common practice to avoid the “noisy” appearance of a spectrum obtained by  
452 fast-Fourier transform (FFT). The recorded signal is subdivided to  $p_n$  segments  
453 and subsequently, the frequency resolution of the resulted spectrum is reduced  
454 by  $p_n$  times, yielding an error of this process of  $\frac{1}{p_n}100\%$ . The optimal number  
455 of segments is selected by trials and for the present case was  $p_n = 8$ . The  
456 smoothing method ensures that the total energy between the measured and the  
457 processed spectrum is conserved. In practice, the smoothing method for the  
458 spectra, as described in the appendix of [46], is the same as the commonly used  
459 Welch without overlapping of the segments. Finally, it was decided to use the  
460 method of [46], since it has no bias on the selection of the overlapping window  
461 function, as with Welch method, and the frequency resolution was sufficient for  
462 the scope of the present study

463 The resulted incident spectra after the reflection analysis and smoothing  
464 are presented in Figure 9. The comparison with the input spectra to the wave  
465 paddle revealed some discrepancies, possibly caused by the calibration and the  
466 imperfect reflection absorption of the wave paddle. The peaks of the mea-  
467 sured spectra were lower than the theoretical and energy was spread to higher  
468 frequencies. Despite these differences, the spectral shape was maintained to  
469 an acceptable degree and the measured incident spectra had on average 20%  
470 higher energy than that of the corresponding input spectra. In the analysis of  
471 the behaviour of the OWCs that follows, the processed incident spectra were  
472 employed for better reliability.

473 Figure 9 also shows that in spite of the different random phases of the ir-  
474 regular waves and the long distance between the WGs used for the reflection  
475 analysis, the obtained incident spectra for all the models were very similar. A  
476 small difference close to the peak frequency was observed for irregular Wave 1,  
477 where the models with the slope appeared to receive more incident energy than  
478 the conventional OWC and U-OWC (Models 1 and 3). The reason for this is  
479 not clear, but it is assumed to be an artefact of the reflection analysis or the  
480 effect of nonlinearities caused by the devices, such as the reflection from the

481 ramp. Similar behaviour can be observed, to a lesser extent, for irregular Wave  
 482 2, while the curves collapse to one for irregular Waves 3 and 4 that have lower  
 483 peak frequencies (see Table 2).

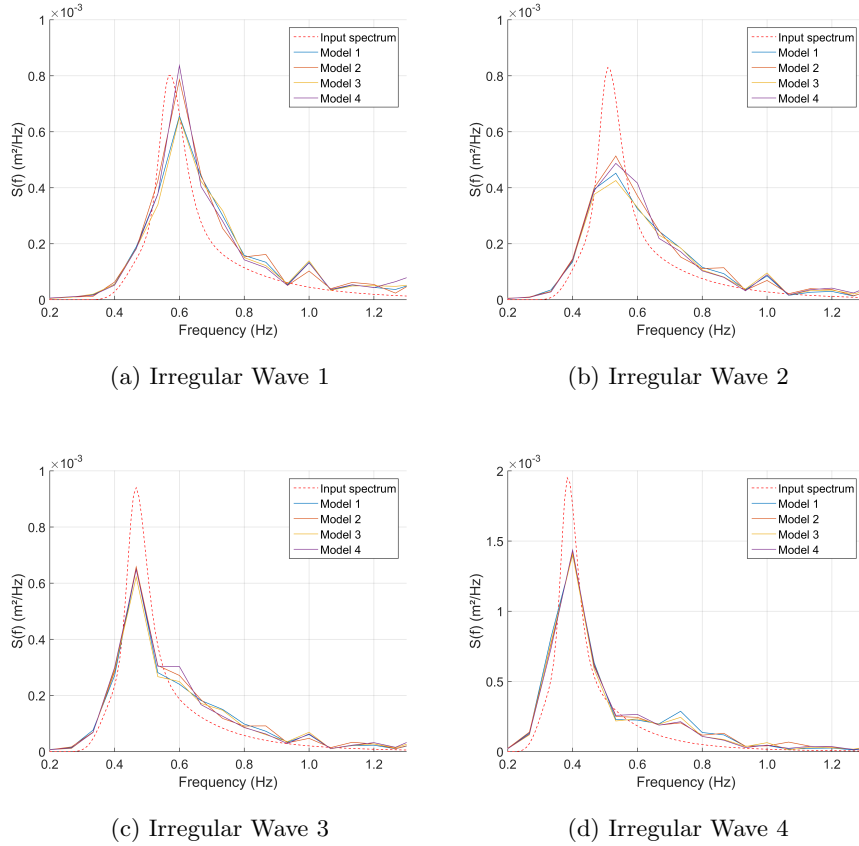


Figure 9: Calculated incident spectra for every model under the four irregular wave conditions.

### 484 3.2.2. Hydrodynamic efficiency

485 Similar to the regular waves, the calculation of the hydrodynamic efficiency  
 486 for the irregular waves ( $C_w^{irr}$ ) requires the incident power of the wave field, which  
 487 can be found by the zeroth spectral moment of the variance energy density of  
 488 the incident spectrum [51] obtained after the reflection analysis. The incident

489 wave power per meter length reads:

$$P_w^{irr} = \rho g \int_0^\infty c_g(\omega) S(\omega) d\omega \quad (9)$$

490 The absorbed power by the OWC ( $P_{abs}^{irr}$ ) is calculated similarly to Equation  
 491 8 for the length of the time series, between the arrival of the first waves at the  
 492 OWC at time  $t_0$  and the end of the signal at time  $t_l$ :

$$P_{abs}^{irr} = \frac{1}{t_{tot}} \int_{t_0}^{t_l} p(t) v(t) S_c dt \quad (10)$$

493  $C_w^{irr}$  can now be found by the ratio of the absorbed energy  $E_{abs}^{irr}$  over the  
 494 incident wave energy  $E_w^{irr}$  between times  $t_0$  and  $t_l$ .

$$C_w^{irr} = \frac{E_{abs}^{irr}}{E_w^{irr}} = \frac{\int_{t_0}^{t_l} p(t) v(t) S_c dt}{w (t_l - t_0) P_w^{irr}} \quad (11)$$

495 Following this procedure, a value of the  $C_w^{irr}$  was calculated for every irreg-  
 496 ular wave and model. To allow comparison, each value of the  $C_w^{irr}$  had to be  
 497 assigned to a representative frequency for every spectrum. A spectrum is com-  
 498 monly represented by its peak frequency ( $f_p$ ), which corresponds to frequency  
 499 of the maximum energy density. However, the relatively low resolution of the  
 500 smoothed spectra (see Figure 9) can introduce some errors in the estimation  
 501 of  $f_p$ . Therefore, it was preferred to calculate  $f_p$  from the spectral moments  
 502 for greater accuracy. At first, the mean frequency of the spectrum  $f_{mean}$  was  
 503 calculated as the ratio between the first and the zeroth spectral moments, as  
 504 shown in Equation 12.  $f_p$  could be then related to  $f_{mean}$  with Equation 13 for a  
 505 JONSWAP spectrum with  $\gamma = 3.3$  [52]. In some cases presented here,  $\gamma < 3.3$ ,  
 506 however the theoretical value of the coefficient (0.8345) can be taken without  
 507 important loss of accuracy (see Table 3 in [52]).

$$f_{mean} = \frac{m_1}{m_0} = \frac{\int_0^\infty f E(f) df}{\int_0^\infty E(f) df} \quad (12)$$

$$f_p = 0.8345 f_{mean} \quad (13)$$



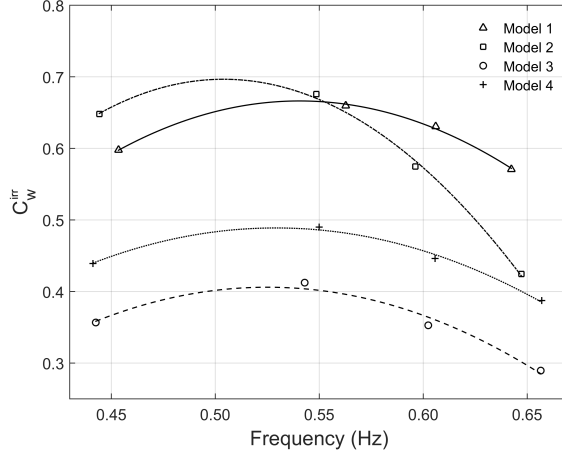


Figure 10: Capture width ratio of the central chamber of each Model for the four irregular waves.

508 Figure 10 shows the comparison between the  $C_w^{irr}$  for the middle chamber of  
 509 each model. A second order polynomial fitting is used to facilitate comparisons.  
 510 Similarly to the regular waves in Figure 7, the U-OWCs (Models 1 and 2) seem  
 511 to be more efficient than the conventional OWC (Models 3 and 4). Moreover, for  
 512 irregular waves, Model 4 appears to be considerably more efficient than Model  
 513 3, possibly because it resonates in higher frequencies, as discussed in Section  
 514 3.1.2. On the other hand, Model 4 does not have better performance for all the  
 515 tests, as it was the case for regular waves. In general, the curvature of the curves  
 516 for irregular waves is smaller than that of regular waves (Figure 7), which can  
 517 be explained by the spread of energy over many frequencies.

518 Even though Figure 10 shows some clear trends in the behaviour of the mod-  
 519 els, it should be noted that these results come from single tests for each irregular  
 520 wave with random phases and more experiments are required to minimise the  
 521 bias of the phases and draw more solid conclusions.

#### 522 4. Conclusions

523 In this study, four multi-chamber designs of OWCs were examined with a  
524 PTO for energy generation and without a PTO, as absorbing seawalls. Re-  
525 garding the performance of the devices with the PTO, the experimental results  
526 confirmed that the U-OWC, as suggested by Boccotti [30], is superior to the  
527 conventional OWC designs. The new U-OWC design with the slope, as sug-  
528 gested here, appeared to have comparatively good performance, which in most  
529 cases was better than all the other models. Moreover, the proposed modifica-  
530 tion to the conventional OWC by including a toe protection unit enhanced the  
531 performance of the classic model. Additionally, the response of the devices was  
532 examined in terms of RAO inside each chamber and run-up on the front wall of  
533 the device. The latter is associated with over-topping, which is a major design  
534 consideration for piers and breakwaters of ports. The present results demon-  
535 strated that for most of the wave conditions tested the presence of the OWC  
536 can reduce the run-up compared with vertical wall breakwaters. The potential  
537 merits for using OWC in classic coastal structures can foster the expansion of  
538 MRE on a cost-sharing basis with coastal protection.

539 Future work should examine the different models in more wave conditions  
540 and with additional instrumentation, in order to draw in-detail conclusions  
541 regarding the effect of the geometric modifications. As demonstrated by the  
542 present study, the geometry of the OWC can have significant impact on its be-  
543 haviour. In future parametric analyses, other design aspects can be examined,  
544 such as the draught of the front wall and the internal geometry of the chambers.  
545 Different levels of damping and other types of PTOs should also be considered,  
546 since the damping, in combination with the geometry of the OWC, determine  
547 the performance of the device. Ideally, the type and the damping of the PTO  
548 should be tuned for each OWC based on the performance curve and the wave  
549 climate that the device will be deployed in. For the case of embedding OWCs  
550 in piers of ports, the reflection coefficients of the structure, together with the  
551 run-up and overtopping should be studied carefully. Finally, an important de-

552 sign aspect is the behaviour of the individual chambers and their interactions  
553 in unidirectional and oblique waves, as the present results indicated differences  
554 in the chambers' response to regular waves.

## 555 **References**

- 556 [1] P. Boccotti, On a new wave energy absorber, *Ocean Engineering* 30 (9)  
557 (2003) 1191–1200. doi:10.1016/S0029-8018(02)00102-6.  
558 URL [http://linkinghub.elsevier.com/retrieve/pii/  
559 S0029801802001026](http://linkinghub.elsevier.com/retrieve/pii/S0029801802001026)
- 560 [2] A. Clément, P. McCullen, A. Falcão, A. Fiorentino, F. Gardner, K. Ham-  
561 marlund, G. Lemonis, T. Lewis, K. Nielsen, S. Petroncini, M. T. Pontes,  
562 P. Schild, B. O. Sjöström, H. C. Sørensen, T. Thorpe, Wave energy in Eu-  
563 rope: Current status and perspectives, *Renewable and Sustainable Energy*  
564 *Reviews* 6 (5) (2002) 405–431. doi:10.1016/S1364-0321(02)00009-6.
- 565 [3] E. Enferad, D. Nazarpour, *New Developments in Renewable Energy*,  
566 Intech, 2013, Ch. 12. doi:10.5772/53806.  
567 URL [http://www.intechopen.com/books/  
568 new-developments-in-renewable-energy/  
569 ocean-s-renewable-power-and-review-of-technologies-case-study-waves](http://www.intechopen.com/books/new-developments-in-renewable-energy/ocean-s-renewable-power-and-review-of-technologies-case-study-waves)
- 570 [4] R. H. Charlier, M.-C. Chaineux, C. W. Finkl, A. C. Thys, Power from  
571 Artic waters, in: *International Congress of Polar Science*, no. 42, 2012, pp.  
572 93–102.
- 573 [5] E. Medina-Lopez, W. Allsop, A. Dimakopoulos, T. Bruce, Conjectures on  
574 the Failure of the OWC Breakwater at Mutriku, in: *Coastal Structures &*  
575 *Solutions To Coastal Disasters Joint Conference*, 2015, pp. 1–12.
- 576 [6] Y. Torre-Enciso, J. Marqués, L. I. Lopez de Aguilera, Mutriku . Lessons  
577 learnt, in: *3rd International Conference on Ocean Energy*, Bilbao, Spain,  
578 2010.

- 579 [7] J. Weber, WEC Technology Readiness and Performance Matrix finding  
580 the best research technology development trajectory, in: 4 th International  
581 Conference on Ocean Energy, Dublin, Ireland, 2012.
- 582 [8] C. B. Boake, T. J. T. Whittaker, M. Folley, H. Ellen, Overview and Initial  
583 Operational Experience of the LIMPET Wave Energy Plant, Vol. 3, 2002,  
584 pp. 586–594.
- 585 [9] A. Pecher, J. P. Kofoed, I. L. Crom, F. Neumann, E. d. B. Azevedo,  
586 Performance assessment of the Pico OWC power plant following the  
587 EquiMar Methodology, in: Proceedings of 21st International Offshore and  
588 Polar Engineering Conference, Vol. 8, 2011, pp. 548–556.  
589 URL [http://e-book.lib.sjtu.edu.cn/isope2011/data/papers/  
590 11TPC-447Pecher.pdf](http://e-book.lib.sjtu.edu.cn/isope2011/data/papers/11TPC-447Pecher.pdf)
- 591 [10] A. F. O. Falcão, J. C. C. Henriques, Model-prototype similarity of  
592 oscillating-water-column wave energy converters, International Journal of  
593 Marine Energy 6 (2014) 18–34. doi:10.1016/j.ijome.2014.05.002.
- 594 [11] M. E. McCormick, Analysis of a Wave Energy Conversion Buoy, Journal  
595 of Hydronautics 8 (3) (1974) 77–82.
- 596 [12] A. F. O. Falcão, Modelling of Wave Energy Conversion, Tech. rep. (2013).  
597 URL [https://fenix.tecnico.ulisboa.pt/downloadFile/  
598 3779580606646/Chapter%25201%25282014%2529.pdf](https://fenix.tecnico.ulisboa.pt/downloadFile/3779580606646/Chapter%25201%25282014%2529.pdf)
- 599 [13] D. Stagonas, G. Müller, N. Maravelakis, D. Magagna, D. Warbrick, Com-  
600 posite seawalls for wave energy conversion: 2D experimental results, in:  
601 3rd International Conference on Ocean Energy, Bilbao, Spain, 2010.
- 602 [14] T. Hammons, Energy Potential of the Oceans in Europe and North Amer-  
603 ica: Tidal, Wave, Currents, Otec and Offshore Wind, International Journal  
604 of Power and Energy Systems 28 (4). doi:10.2316/Journal.203.2008.  
605 4.203-4142.

- 606 [15] A. Sarmiento, Wave flume experiments on two-dimensional oscillating water  
607 column wave energy devices, *Experiments in Fluids* 12 (4-5) (1992) 286–  
608 292. doi:10.1007/BF00187307.  
609 URL <http://dx.doi.org/10.1007/BF00187307>
- 610 [16] M. T. Morris-Thomas, R. J. Irvin, K. P. Thiagarajan, An Investigation Into  
611 the Hydrodynamic Efficiency of an Oscillating Water Column, *Journal of*  
612 *Offshore Mechanics and Arctic Engineering* 129 (4) (2007) 273–278. doi:  
613 10.1115/1.2426992.
- 614 [17] Y. Zhang, Q.-P. Zou, D. Greaves, Airwater two-phase flow modelling of hy-  
615 drodynamic performance of an oscillating water column device, *Renewable*  
616 *Energy* 41 (2012) 159–170. doi:10.1016/j.renene.2011.10.011.  
617 URL <http://dx.doi.org/10.1016/j.renene.2011.10.011>
- 618 [18] Y. Luo, J. R. Nader, P. Cooper, S. P. Zhu, Nonlinear 2D analysis of the  
619 efficiency of fixed Oscillating Water Column wave energy converters, *Re-*  
620 *newable Energy* 64 (2014) 255–265. doi:10.1016/j.renene.2013.11.007.
- 621 [19] D.-Z. Ning, J. Shi, Q.-P. Zou, B. Teng, Investigation of hydrodynamic  
622 performance of an OWC (oscillating water column) wave energy device  
623 using a fully nonlinear HOBEM (higher-order boundary element method),  
624 *Energy* 83 (2015) 177–188. doi:10.1016/j.energy.2015.02.012.  
625 URL [http://linkinghub.elsevier.com/retrieve/pii/  
626 S0360544215001644](http://linkinghub.elsevier.com/retrieve/pii/S0360544215001644)
- 627 [20] D. Evans, R. Porter, Hydrodynamic characteristics of an oscillating water  
628 column device, *Applied Ocean Research* 17 (3) (1995) 155–164. doi:10.  
629 1016/0141-1187(95)00008-9.
- 630 [21] P. Boccotti, Caisson breakwaters embodying an OWC with a small opening  
631 - Part I: Theory, *Ocean Engineering* 34 (5-6) (2007) 806–819. doi:10.  
632 1016/j.oceaneng.2006.04.006.

- 633 [22] G. Malara, F. Arena, Analytical modelling of an U-Oscillating Water Col-  
634 umn and performance in random waves, *Renewable Energy* 60 (2013) 116–  
635 126. doi:10.1016/j.renene.2013.04.016.  
636 URL <http://dx.doi.org/10.1016/j.renene.2013.04.016>
- 637 [23] I. Morrison, C. Greated, Oscillating water Column Modelling, in: *Coastal*  
638 *Engineering Proceedings*, Vol. 1, 1992, pp. 502–511.
- 639 [24] I. Lopez, A. Castro, G. Iglesias, Hydrodynamic performance of an oscil-  
640 lating water column wave energy converter by means of particle imaging  
641 velocimetry, *Energy* 83 (2015) 89–103. doi:10.1016/j.energy.2015.01.  
642 119.
- 643 [25] K. Ram, M. Faizal, M. Rafiuddin Ahmed, Y.-H. Lee, Experimental studies  
644 on the flow characteristics in an oscillating water column device, *Journal*  
645 *of Mechanical Science and Technology* 24 (10) (2010) 2043–2050. doi:  
646 10.1007/s12206-010-0621-z.
- 647 [26] M. Folley, T. Whittaker, Validating a spectral-domain model of an OWC  
648 using physical model data, *International Journal of Marine Energy* 2 (2013)  
649 1–11. doi:10.1016/j.ijome.2013.05.003.  
650 URL <http://dx.doi.org/10.1016/j.ijome.2013.05.003>
- 651 [27] I. López, B. Pereiras, F. Castro, G. Iglesias, Optimisation of turbine-  
652 induced damping for an OWC wave energy converter using a RANS-VOF  
653 numerical model, *Applied Energy* 127 (2014) 105–114. doi:10.1016/j.  
654 *apenergy*.2014.04.020.
- 655 [28] A. Iturrioz, R. Guanche, J. Lara, C. Vidal, I. Losada, Validation of Open-  
656 FOAM for Oscillating Water Column three-dimensional modeling, *Ocean*  
657 *Engineering* 107 (2015) 222–236. doi:10.1016/j.oceaneng.2015.07.051.  
658 URL [http://linkinghub.elsevier.com/retrieve/pii/  
659 S0029801815003649](http://linkinghub.elsevier.com/retrieve/pii/S0029801815003649)

- 660 [29] I. Simonetti, L. Cappietti, H. El Safti, H. Oumeraci, Numerical Modelling  
661 of Fixed Oscillating Water Column Wave Energy Conversion Devices:  
662 Toward Geometry Hydraulic Optimization, in: Proceedings of the ASME  
663 34th International Conference on Ocean, Offshore and Arctic Engineering  
664 OMAE2015, 2015. doi:10.1115/OMAE2015-42056.  
665 URL [http://www.scopus.com/inward/record.url?eid=2-s2.  
666 0-84947724837{&}partnerID=tZ0tx3y1](http://www.scopus.com/inward/record.url?eid=2-s2.0-84947724837&partnerID=tZ0tx3y1)
- 667 [30] P. Boccotti, Comparison between a U-OWC and a conventional OWC,  
668 Ocean Engineering 34 (5-6) (2007) 799–805. doi:10.1016/j.oceaneng.  
669 2006.04.005.
- 670 [31] T. Vyzikas, S. Deshoulières, O. Giroux, M. Barton, D. Greaves, Numerical  
671 study of fixed Oscillating Water Column with RANS-type two-phase CFD  
672 model, Renewable Energy(Under second revision).
- 673 [32] K. Günaydin, M. S. Kabdali, Investigation of  $\Pi$ -type breakwaters perfor-  
674 mance under regular and irregular waves, Ocean Engineering 34 (7) (2007)  
675 1028–1043. doi:10.1016/j.oceaneng.2006.03.015.
- 676 [33] P. Boccotti, Design of breakwater for conversion of wave energy into elec-  
677 trical energy, Ocean Engineering 51 (2012) 106–118. doi:10.1016/j.  
678 oceaneng.2012.05.011.
- 679 [34] P. Boccotti, P. Filianoti, V. Fiamma, F. Arena, Caisson breakwaters em-  
680 bodying an OWC with a small opening-Part II: A small-scale field ex-  
681 periment, Ocean Engineering 34 (5-6) (2007) 820–841. doi:10.1016/j.  
682 oceaneng.2006.04.016.
- 683 [35] F. Arena, A. Romolo, G. Malara, A. Ascanelli, S. Ghiretti, A New U-OWC  
684 Device to Produce Electrical Power from Ocean Waves : Some Applica-  
685 tions to Italian Coasts, in: ICE Conference Coasts, Marine Structures and  
686 Breakwaters 2013, Edinburgh, UK, 2013.

- 687 [36] K. Ümit Monk, Forecasting for control and environmental impacts of wave  
688 energy converters, Ph.D. thesis (2015). doi:10.1029/2003GL016963.
- 689 [37] P. R. Teixeira, D. P. Davyt, E. Didier, R. Ramalhais, Numerical  
690 simulation of an oscillating water column device using a code  
691 based on Navier Stokes equations, Energy 61 (2013) 513–530.  
692 doi:10.1016/j.energy.2013.08.062.  
693 URL [http://linkinghub.elsevier.com/retrieve/pii/  
694 S0360544213007512](http://linkinghub.elsevier.com/retrieve/pii/S0360544213007512)
- 695 [38] P. M. Koola, M. Ravindran, P. A. A. Narayana, Model Studies of Oscil-  
696 lating Water Column Wave-Energy Device, Journal of Energy Engineering  
697 121 (1) (1995) 14–27. doi:10.1061/(ASCE)0733-9402(1995)121:1(14).
- 698 [39] Coastal, Ocean and Sediment Transport (COAST) Laboratory, [Online  
699 accessed 04-September-2015].  
700 URL <http://www.plymouth.ac.uk/coast>
- 701 [40] G. Payne, Guidance for the experimental tank testing of wave energy  
702 converters, Tech. rep. (2008).  
703 URL [http://www.supergen-marine.org.uk/drupal/files/reports/  
704 WEC\\_tank\\_testing.pdf](http://www.supergen-marine.org.uk/drupal/files/reports/WEC_tank_testing.pdf)
- 705 [41] The wells air turbine for wave energy conversion.
- 706 [42] F. He, Z. Huang, Hydrodynamic performance of pile-supported OWC-type  
707 structures as breakwaters: An experimental study, Ocean Engineering 88  
708 (2014) 618–626. doi:10.1016/j.oceaneng.2014.04.023.  
709 URL [http://linkinghub.elsevier.com/retrieve/pii/  
710 S0029801814001620](http://linkinghub.elsevier.com/retrieve/pii/S0029801814001620)
- 711 [43] A. Kamath, H. Bihs, Øivind A. Arntsen, Numerical modeling of power take-  
712 off damping in an Oscillating Water Column device, International Journal  
713 of Marine Energy 10 (2015) 1–16. doi:10.1016/j.ijome.2015.01.001.  
714 URL <http://dx.doi.org/10.1016/j.ijome.2015.01.001>



- 715 [44] P. Frigaard, M. Christensen, An absorbing wave-maker based on digital fil-  
716 ters, in: Coastal Engineering Conference. Proceedings of The International  
717 Conference 1, pp. 168–180.
- 718 [45] M. E. McCormick, Ocean Wave Energy Conversion, Dover Publications,  
719 2007.
- 720 [46] L. H. Holthuijsen, Waves in Oceanic and Coastal Waters, Cambridge Uni-  
721 versity Press, 2007.
- 722 [47] K. Hasselmann, T. P. Barnett, E. Bouws, H. Carlson, D. E. Cartwright,  
723 K. Enke, J. A. Ewing, H. Gienapp, D. E. Hasselmann, P. Kruse-  
724 man, A. Meerburg, P. Muller, D. J. Olbers, K. Richter, W. Sell,  
725 H. Walden, Measurements of Wind-Wave Growth and Swell Decay dur-  
726 ing the Joint North Sea Wave Project (JONSWAP), *Ergänzungsheft zur*  
727 *Deutschen Hydrographischen Zeitschrift Reihe A*(8) (12) (1973) p.95. doi :  
728 citeulike-article-id:2710264.
- 729 [48] Channel Coastal Laboratory, [Online accessed 04-April-2015].  
730 URL <http://www.channelcoast.org/>
- 731 [49] M. F. P. Lopes, Experimental development of offshore wave energy con-  
732 verters, Ph.D. thesis, Instituto Superior Tecnico (2011).
- 733 [50] T. E. Baldock, D. J. Simmonds, Separation of incident and reflected waves  
734 over sloping bathymetry, *Coastal Engineering* 38 (3) (1999) 167–176. doi :  
735 10.1016/S0378-3839(99)00046-0.
- 736 [51] R. Takaramoto, M. Kashiwagi, K. Sakai, Wave Energy Absorption in Irreg-  
737 ular Waves by a Floating Body Equipped with Interior Rotating Electric-  
738 Power Generator, *Journal of Ocean and Wind Energy* 1 (3) 129–134.
- 739 [52] D. Carter, Estimation of wave spectra from wave height and period (1982).  
740 URL <http://eprints.soton.ac.uk/14556/>